Supplementary Information

High-efficiency metal selenide as electrocatalyst in separator for lithium-sulfur batteries

Yujuan Hu, Bo Jin,* Hui Liu

Key Laboratory of Automobile Materials, Ministry of Education, and School of Materials Science and Engineering, Jilin University, Changchun 130022, China

* Corresponding author. E-mail: jinbo@jlu.edu.cn (B. Jin)

Supplementary Figures

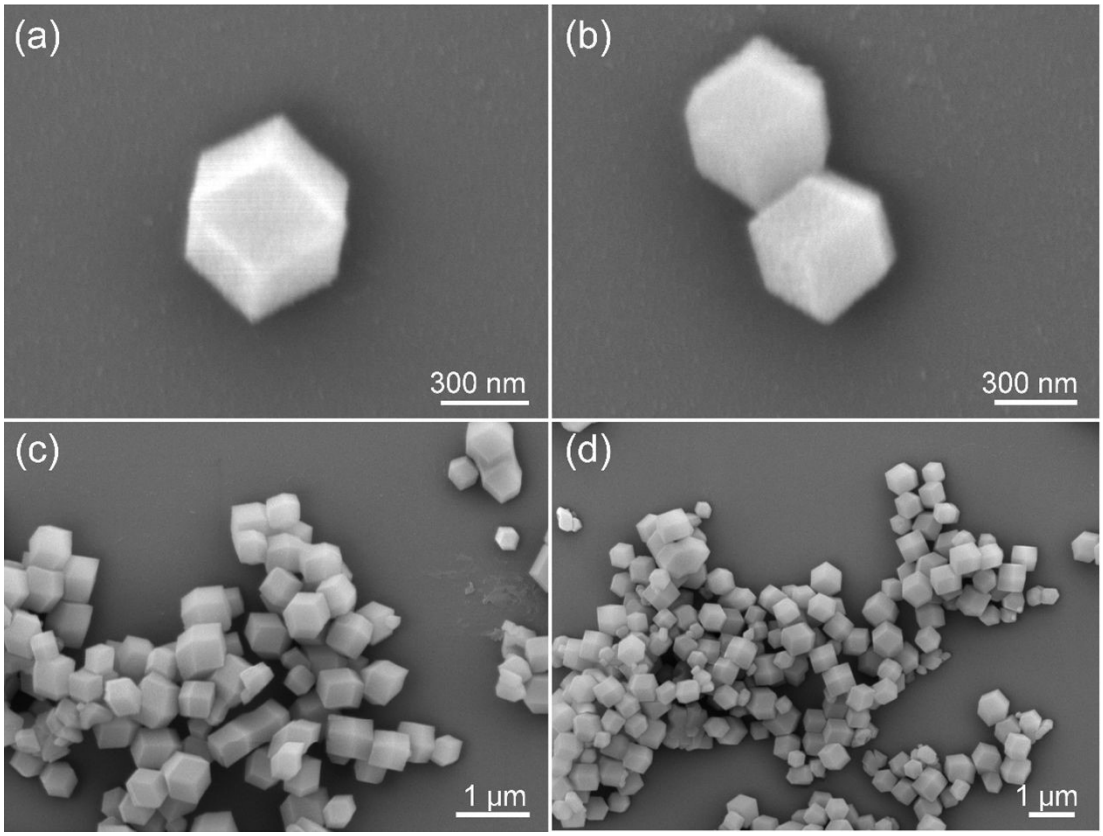

Figure S1 SEM images of ZIF-67 at different magnifications.

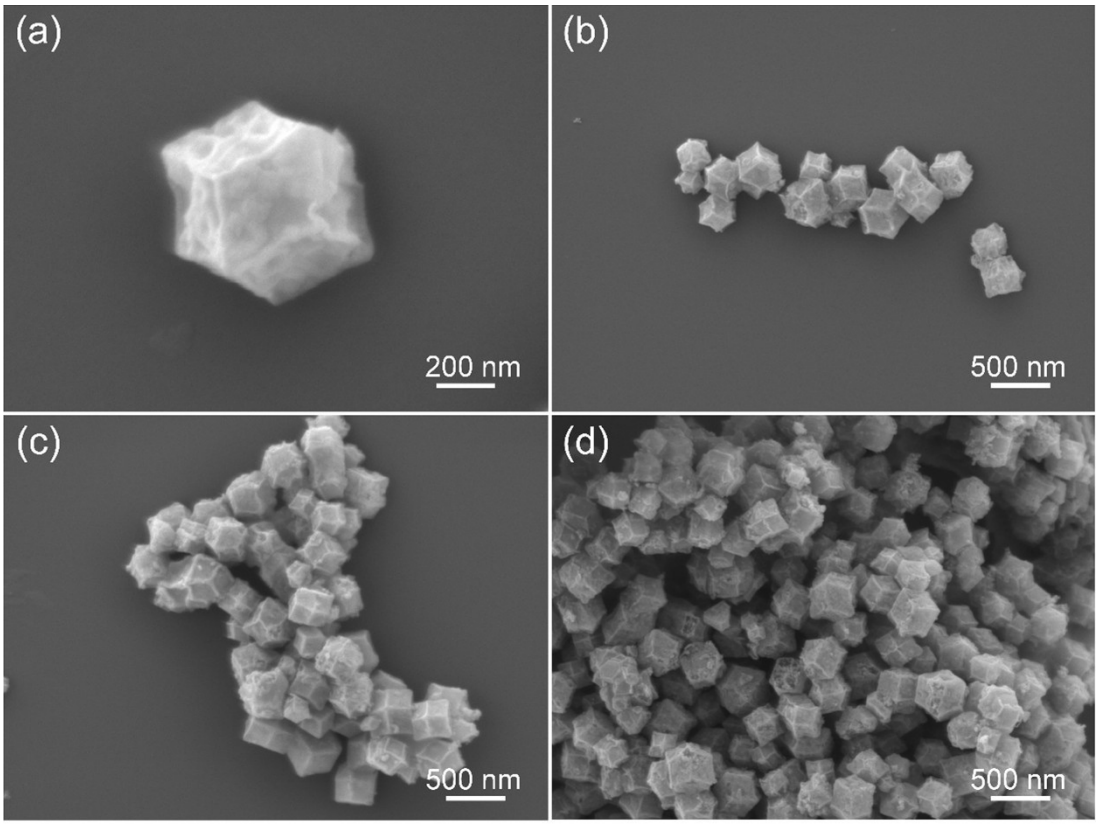

Figure S2 SEM images of Co/NC at (a, b) high magnifications and (c, d) low magnifications.

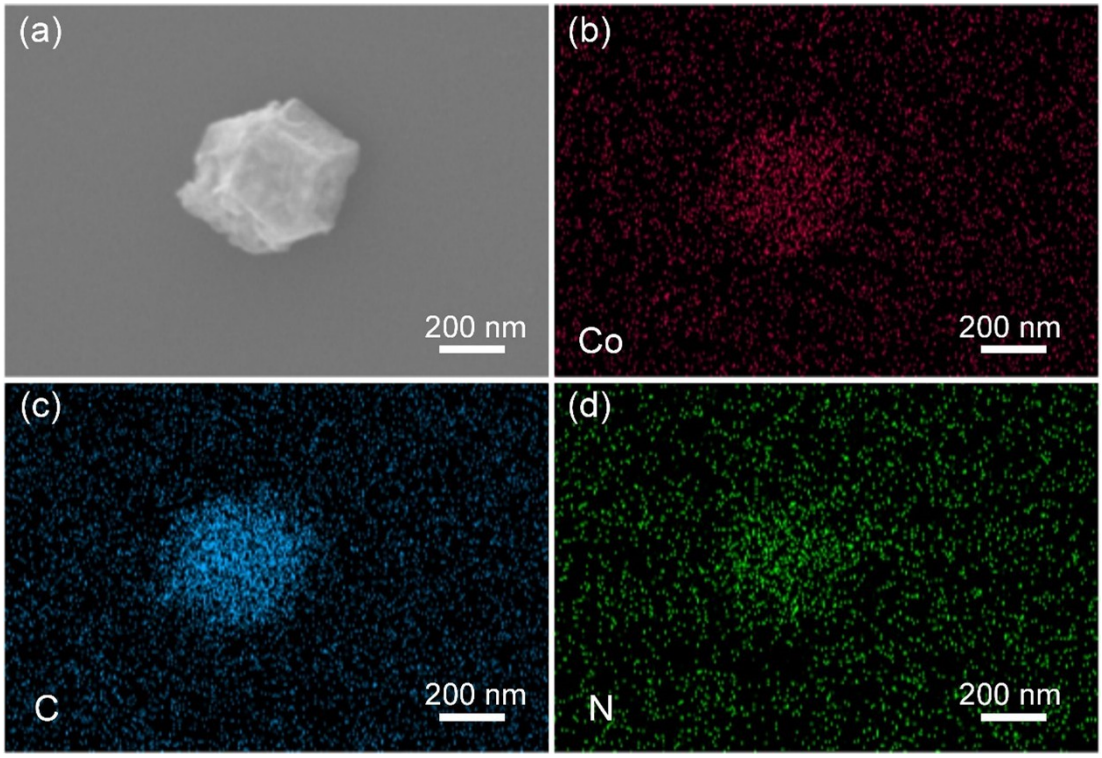

Figure S3 SEM image and (b-d) corresponding elemental mappings of Co/NC.

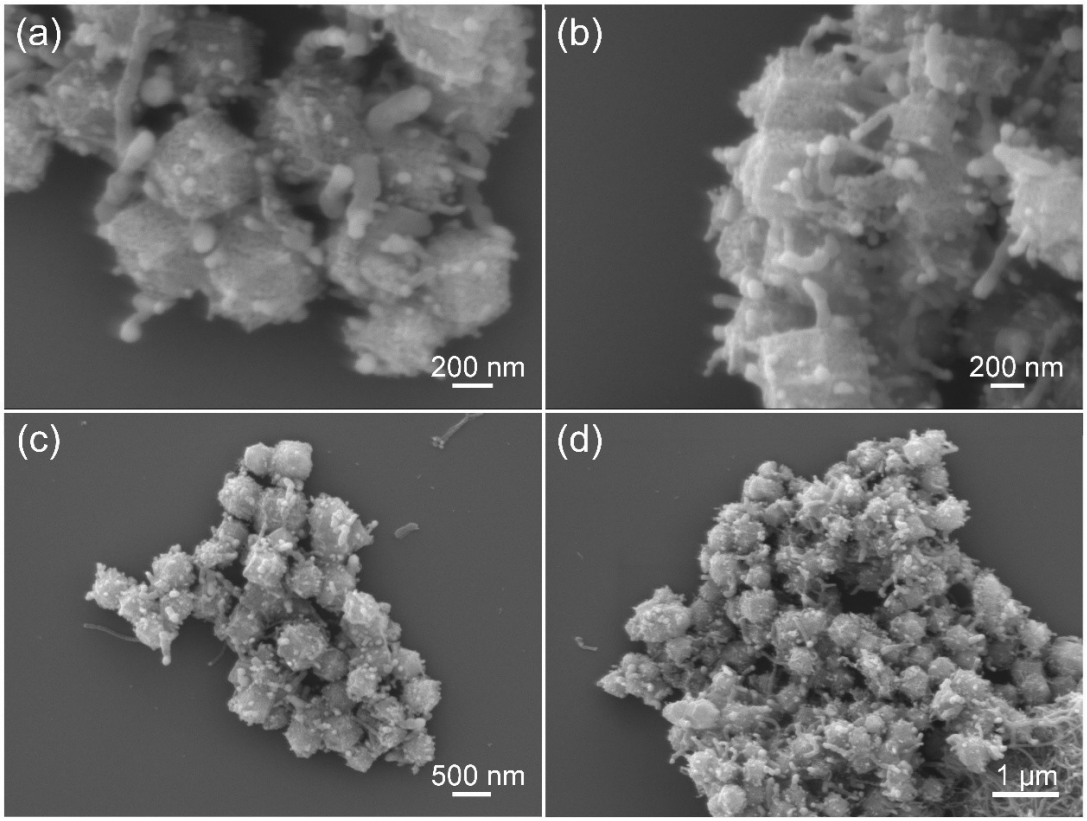

Figure S4 SEM images of Co/NCC at (a, b) high magnifications and (c, d) low magnifications.

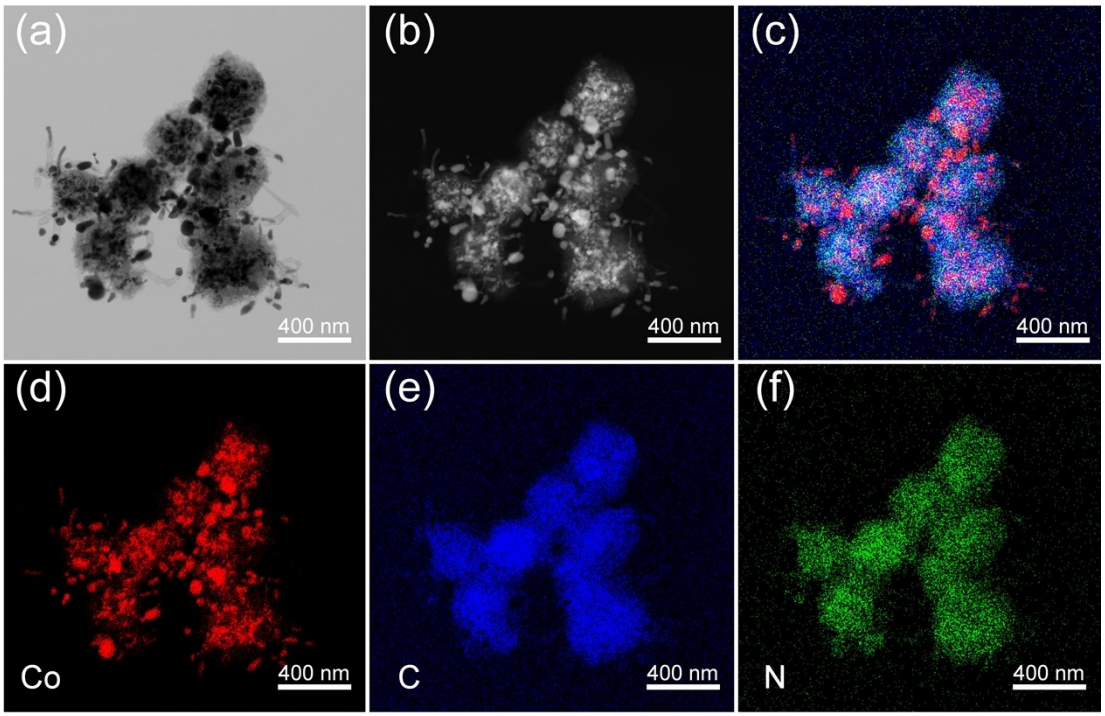

Figure S5 (a) TEM image, (b) HAADF-STEM image, (c) element overlay image, and (d-f) corresponding elemental mappings of Co/NCC.

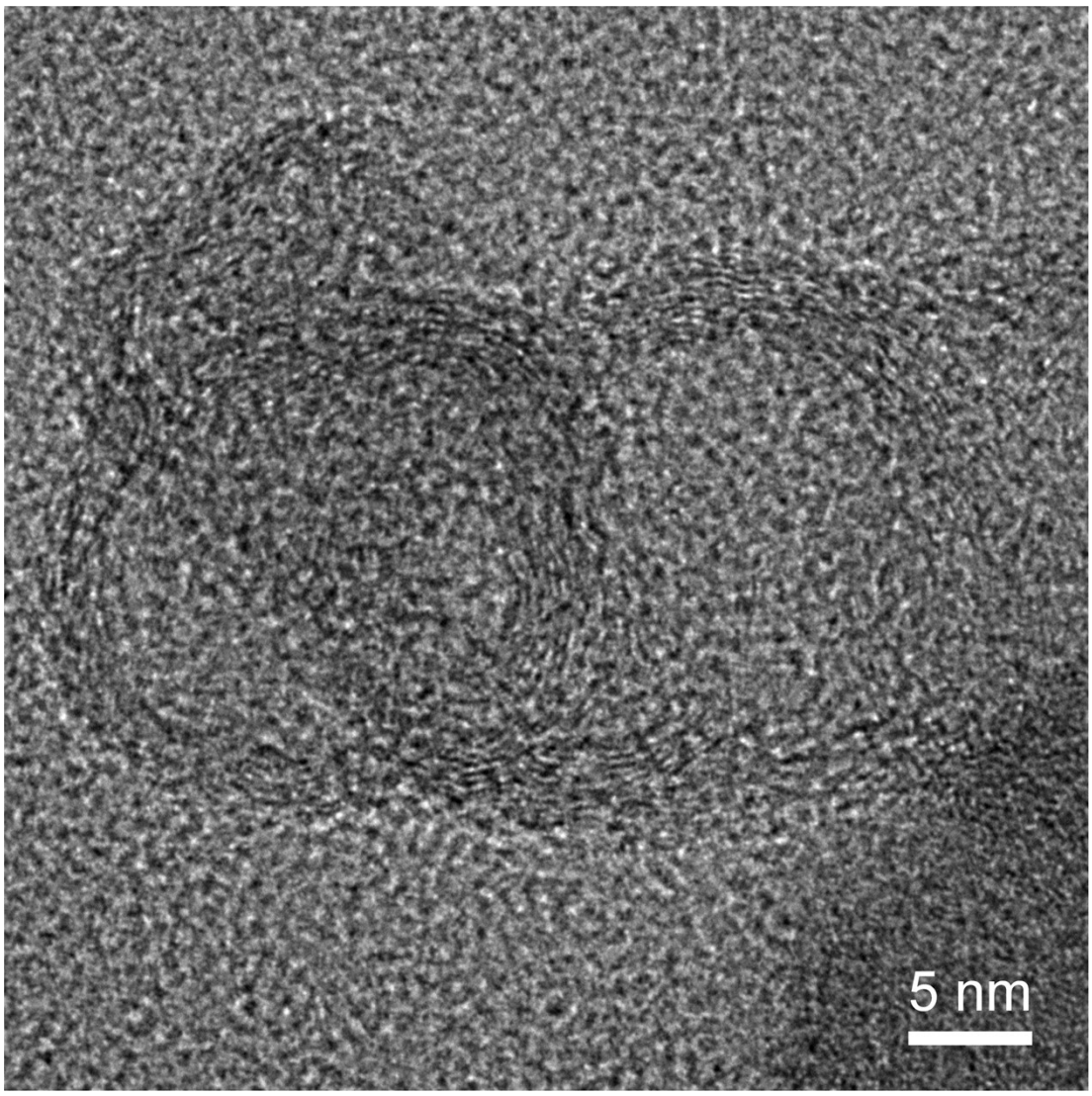

Figure S6 TEM image of CNTs in CoSe/NCC.

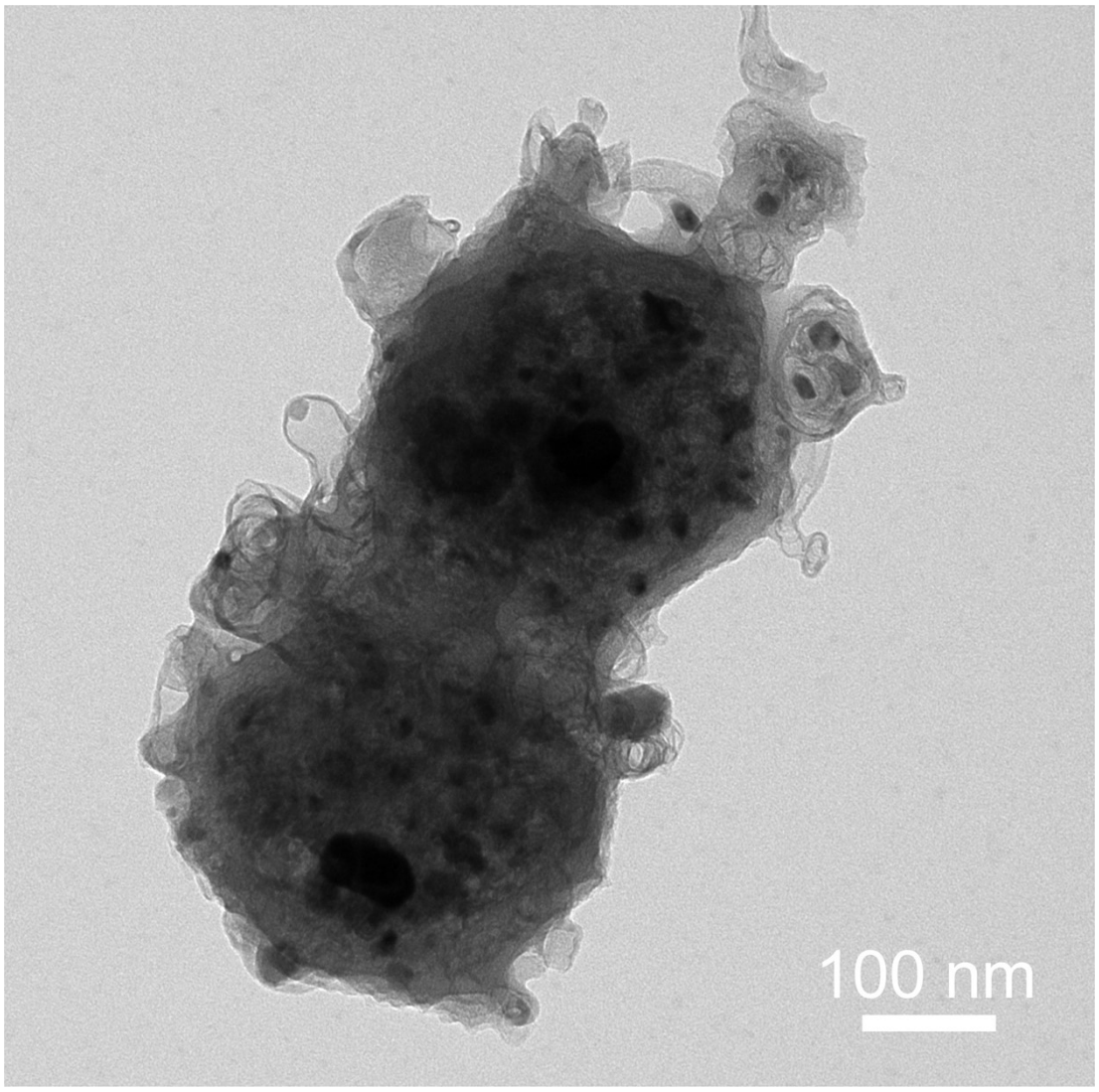

Figure S7 TEM image of CoSe/NCC.

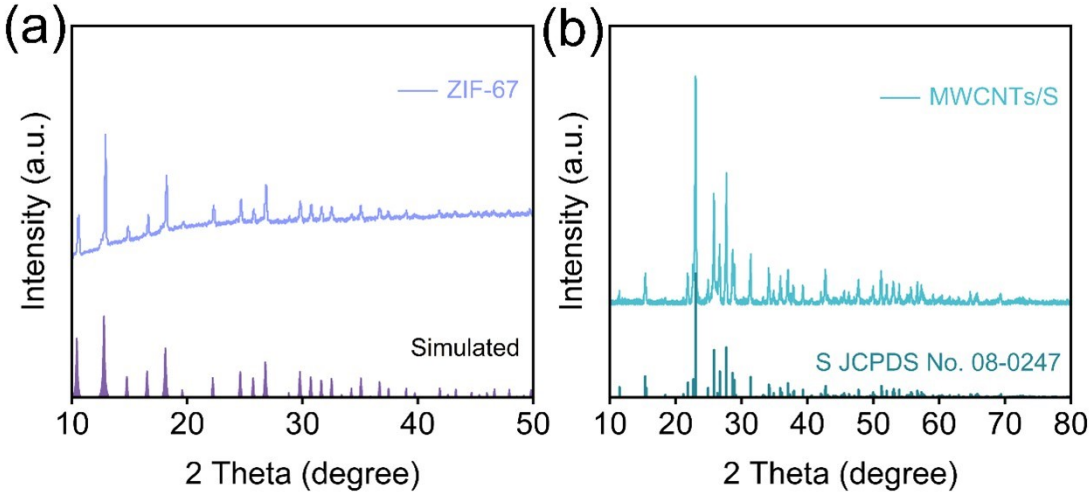

Figure S8 XRD patterns of (a) ZIF-67 and (b) MWCNTs/S.

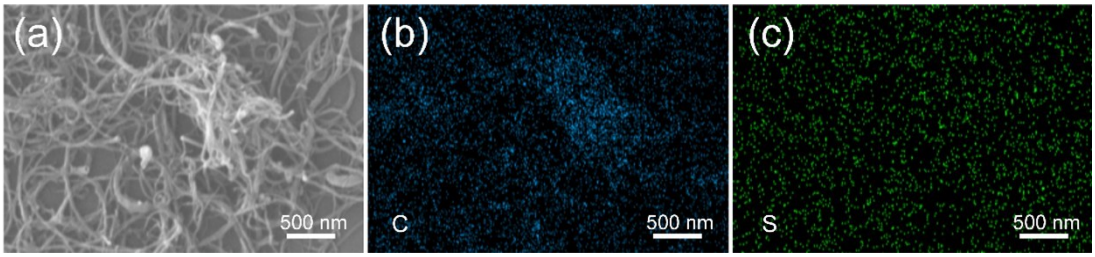

Figure S9 SEM image and (b, c) corresponding elemental mappings of MWCNTs/S.

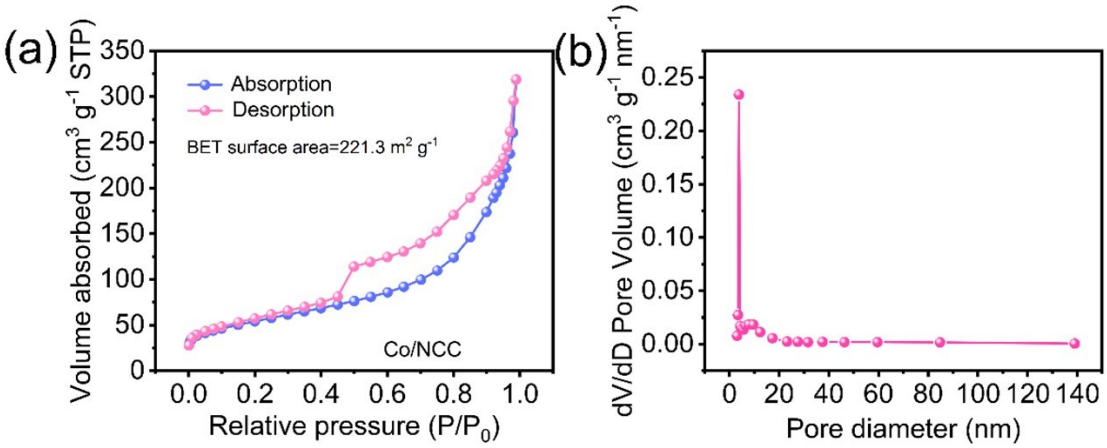

Figure S10 (a) Nitrogen adsorption-desorption isotherm and (b) pore size distribution of Co/NCC.

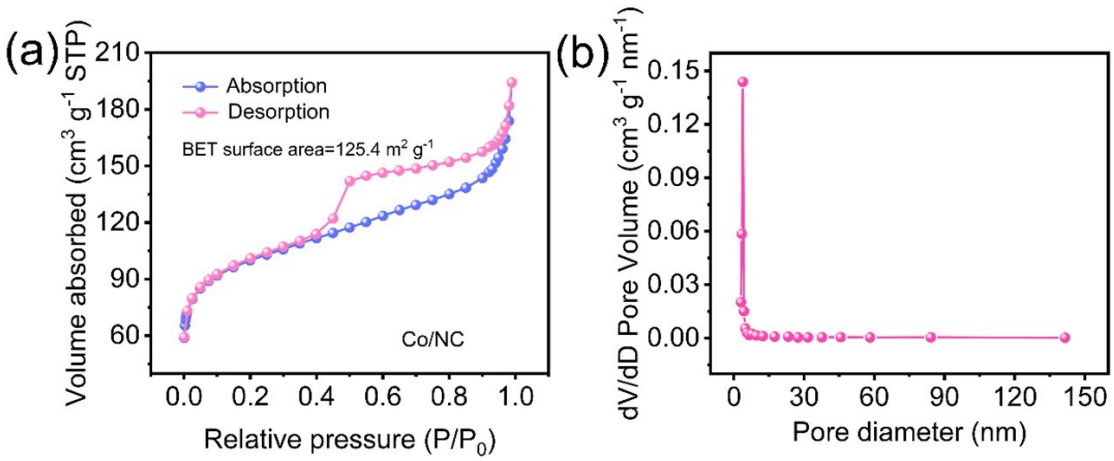

Figure S11 (a) Nitrogen adsorption-desorption isotherm and (b) pore size distribution of Co/NC.

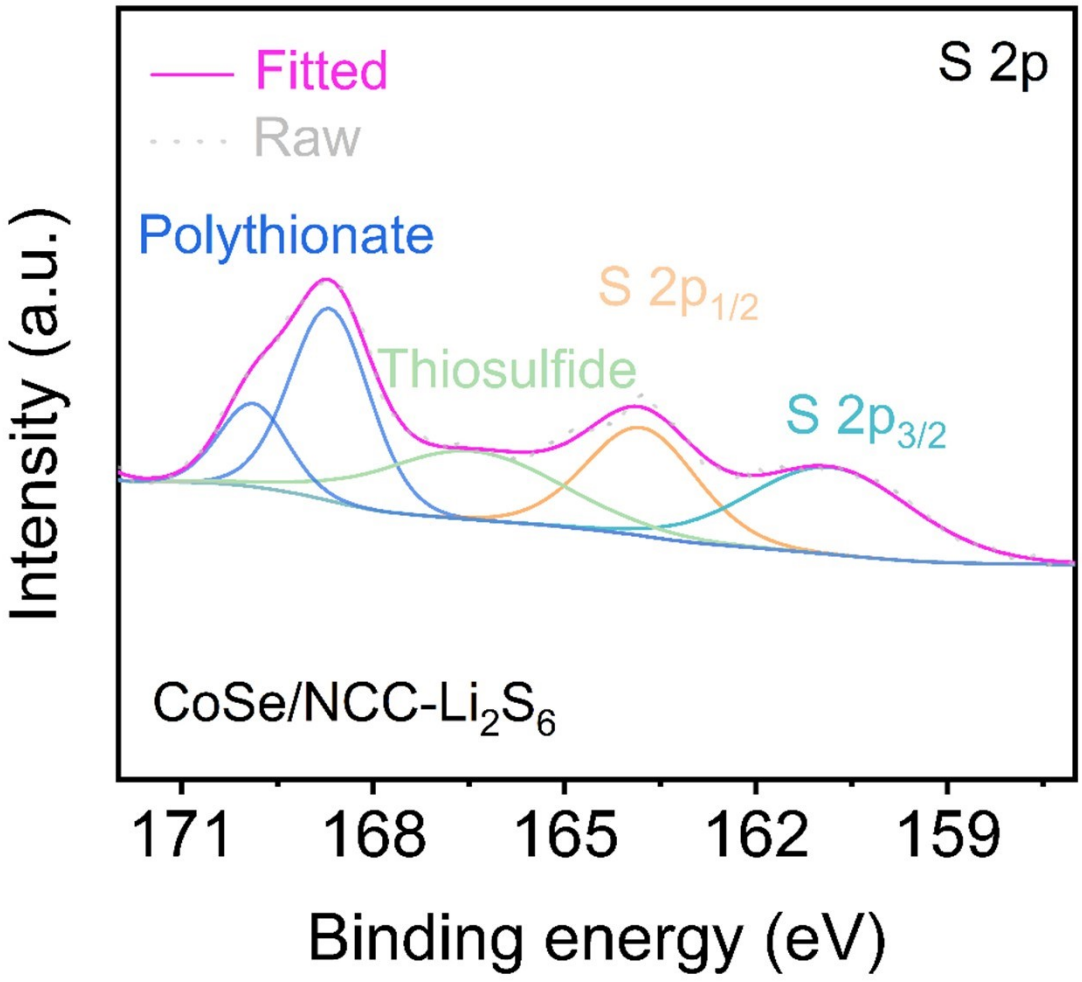

Figure S12 High-resolution XPS spectrum of S 2p in CoSe/NCC-Li_2S_6 solution.

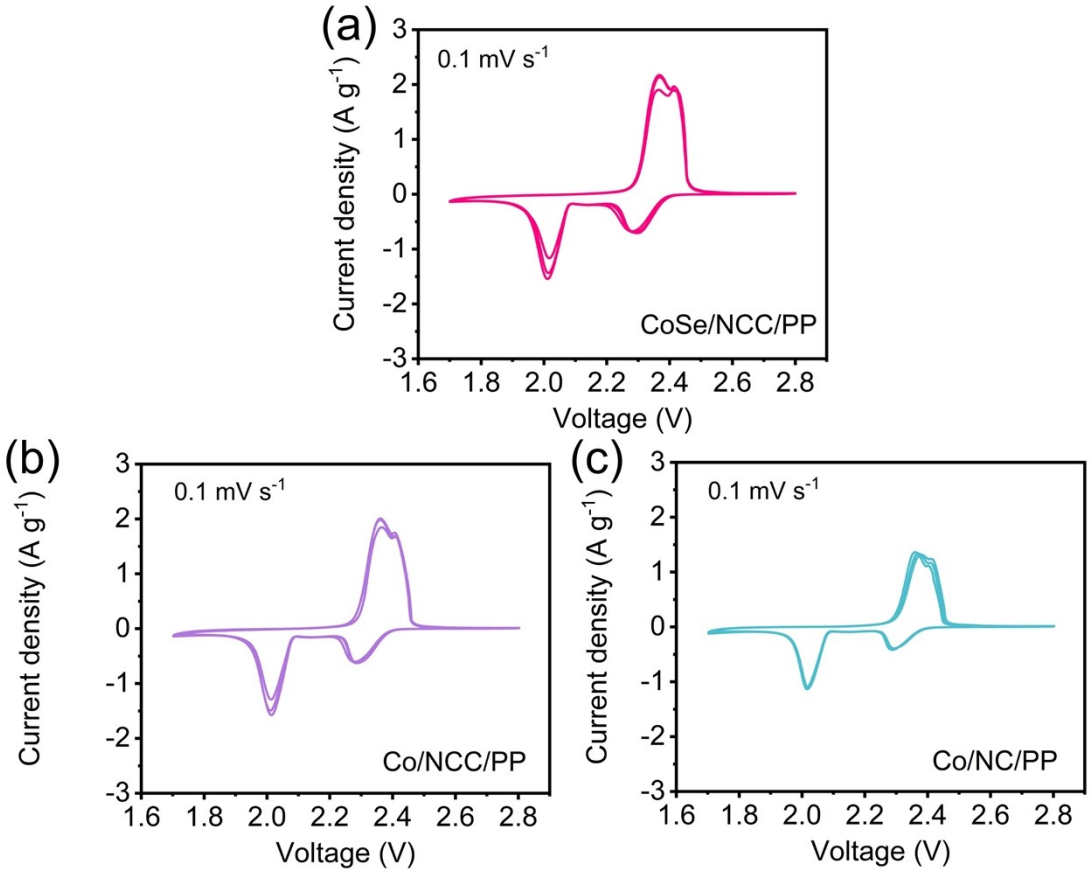

Figure S13 CV curves of LSBs with (a) CoSe/NCC/PP, (b) Co/NCC/PP, and (c) Co/NC-PP separators at the scan rate of 0.1 mVs^{-1} in the first three cycles.

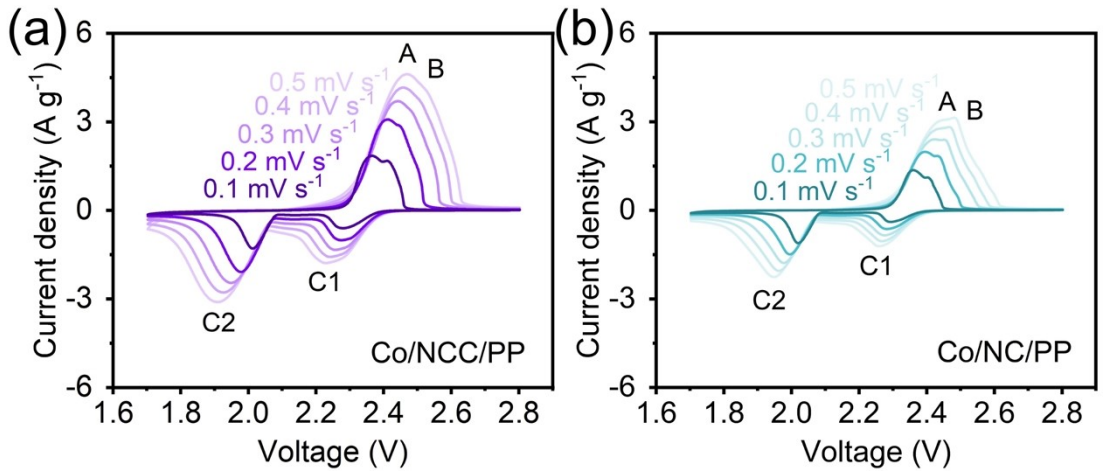

Figure S14 CV curves of LSBs with (a) Co/NCC/PP and (b) Co/NC/PP separators at the scan rates of 0.1-0.5 mV s^{-1}.

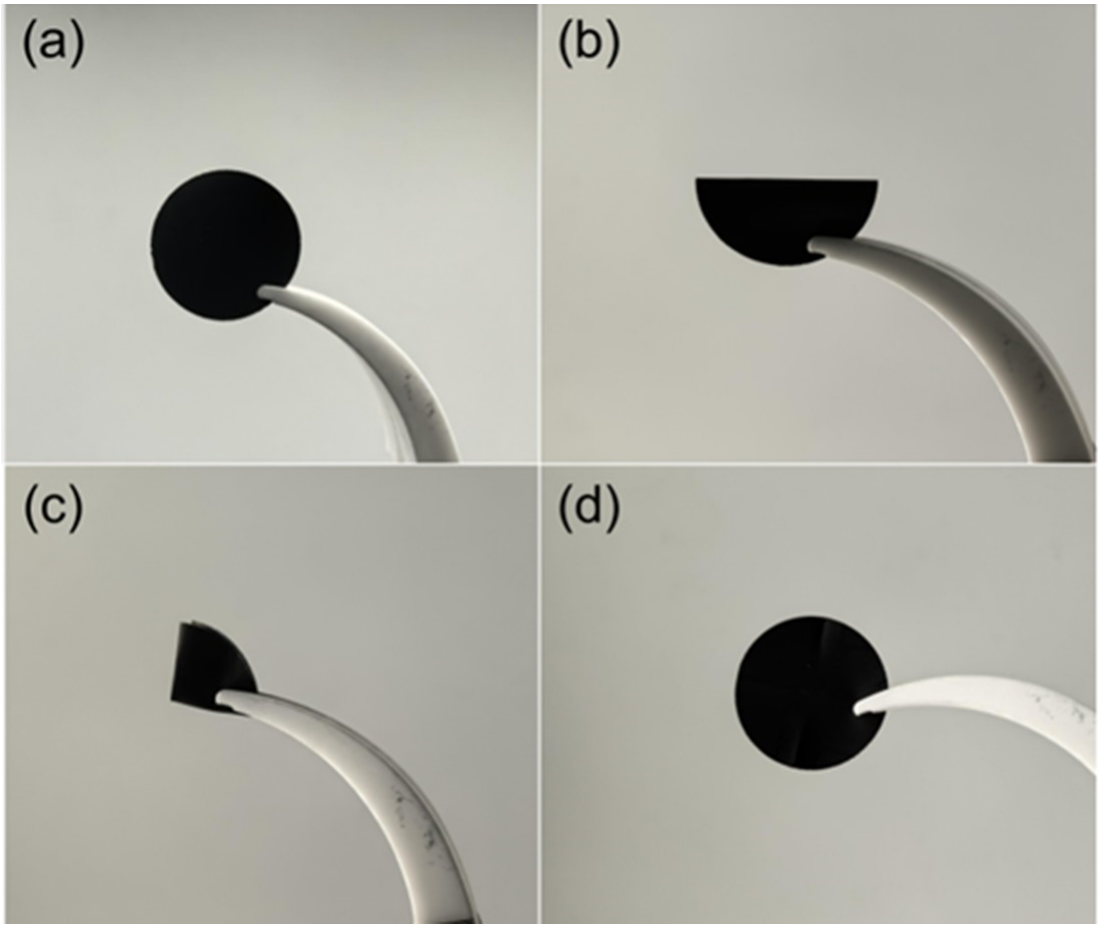

Figure S15 Digital photographs of flexibility tests for CoSe/NCC/PP separator.

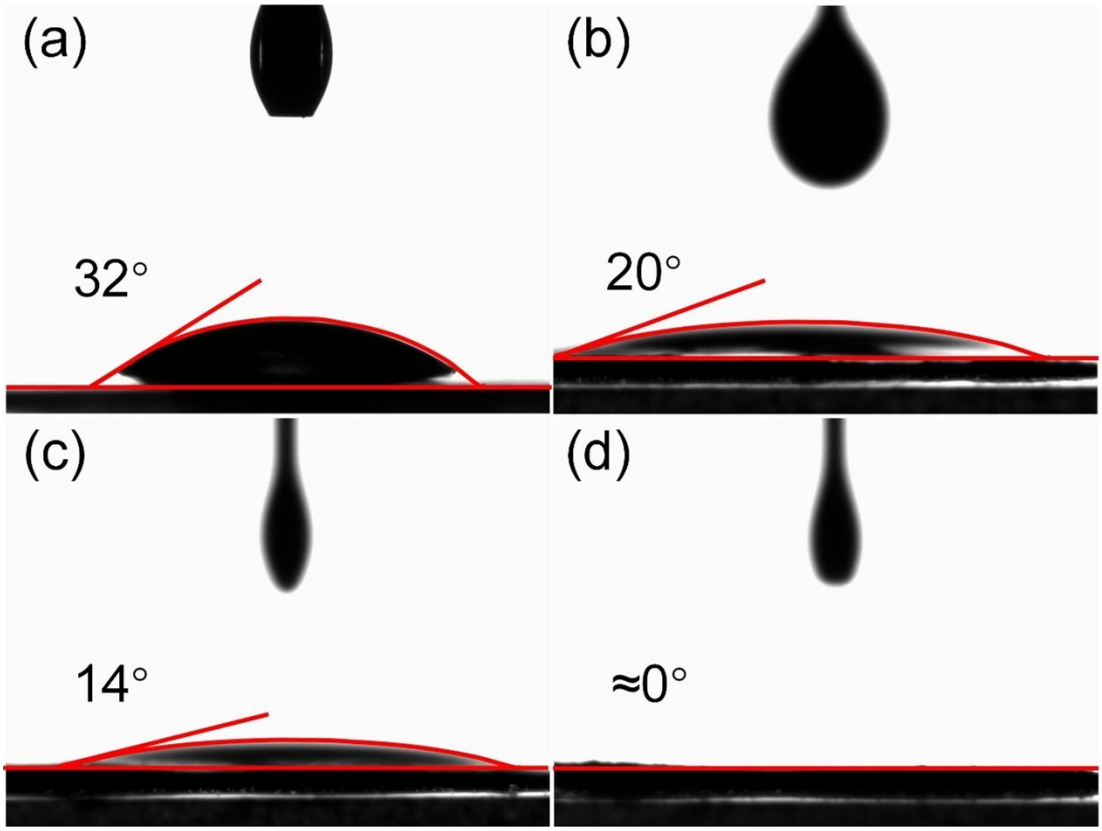

Figure S16 Electrolyte contact angles of (a) PP, (b) Co/NC/PP, (c) Co/NCC/PP, and (d) CoSe/NCC/PP separators.

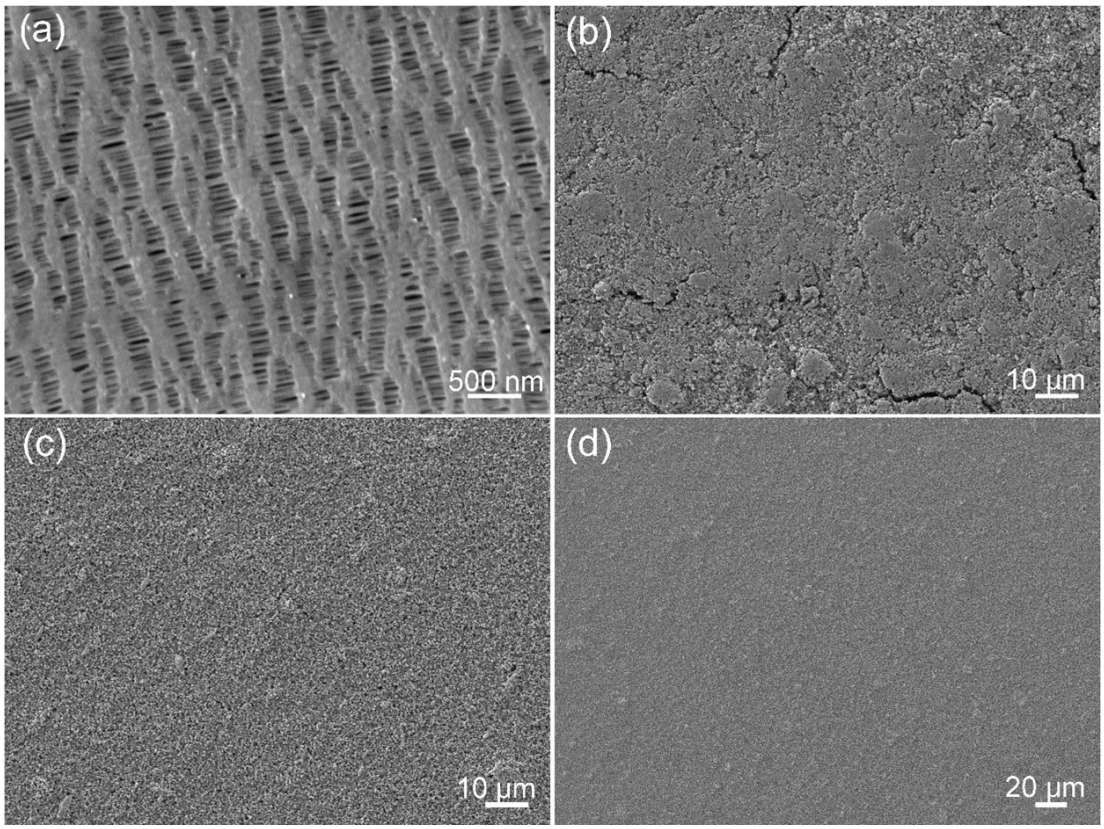

Figure S17 SEM surface images of (a) PP, (b) Co/NC/PP, (C) Co/NCC/PP, and (d) CoSe/NCC/PP separators.

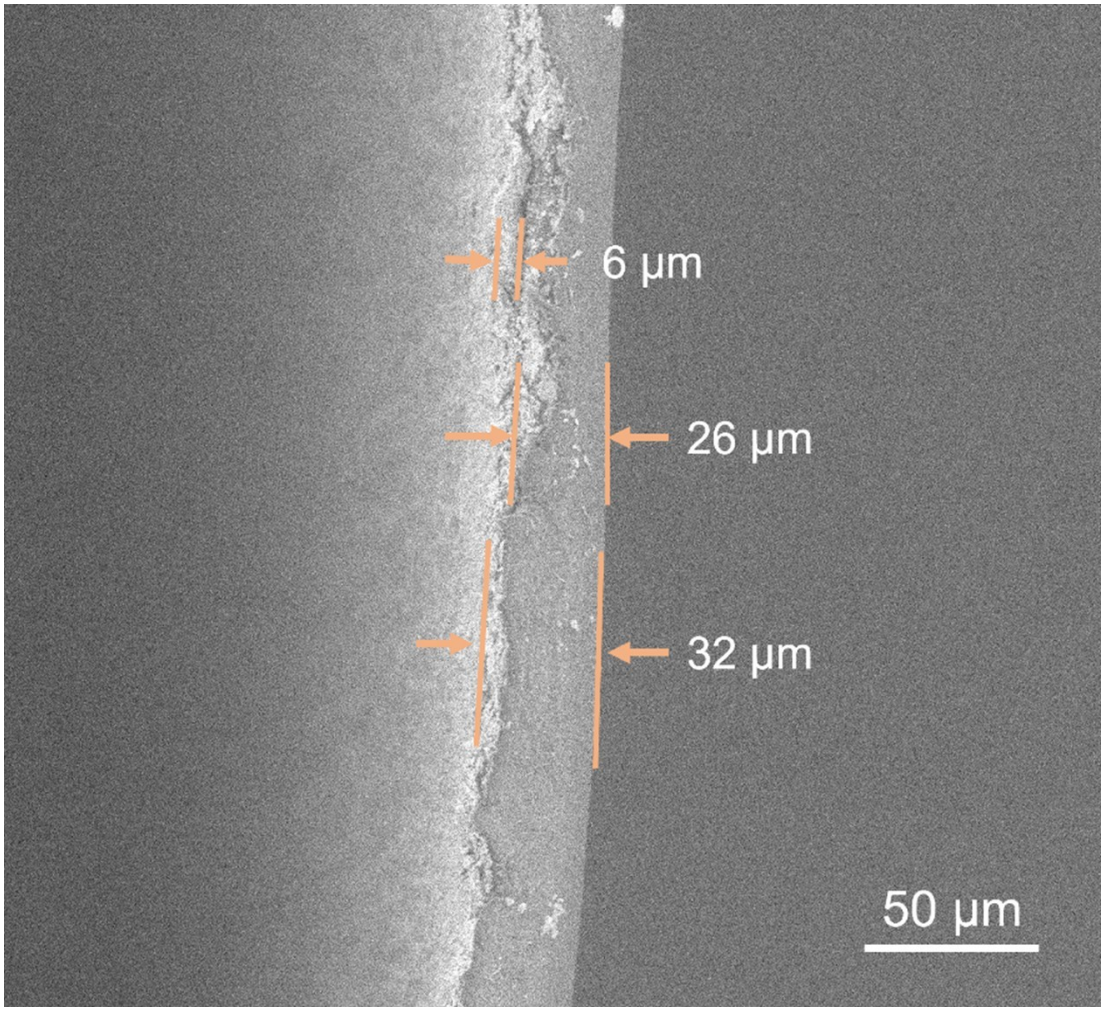

Figure S18 SEM image of cross-section of CoSe/NCC/PP separator.

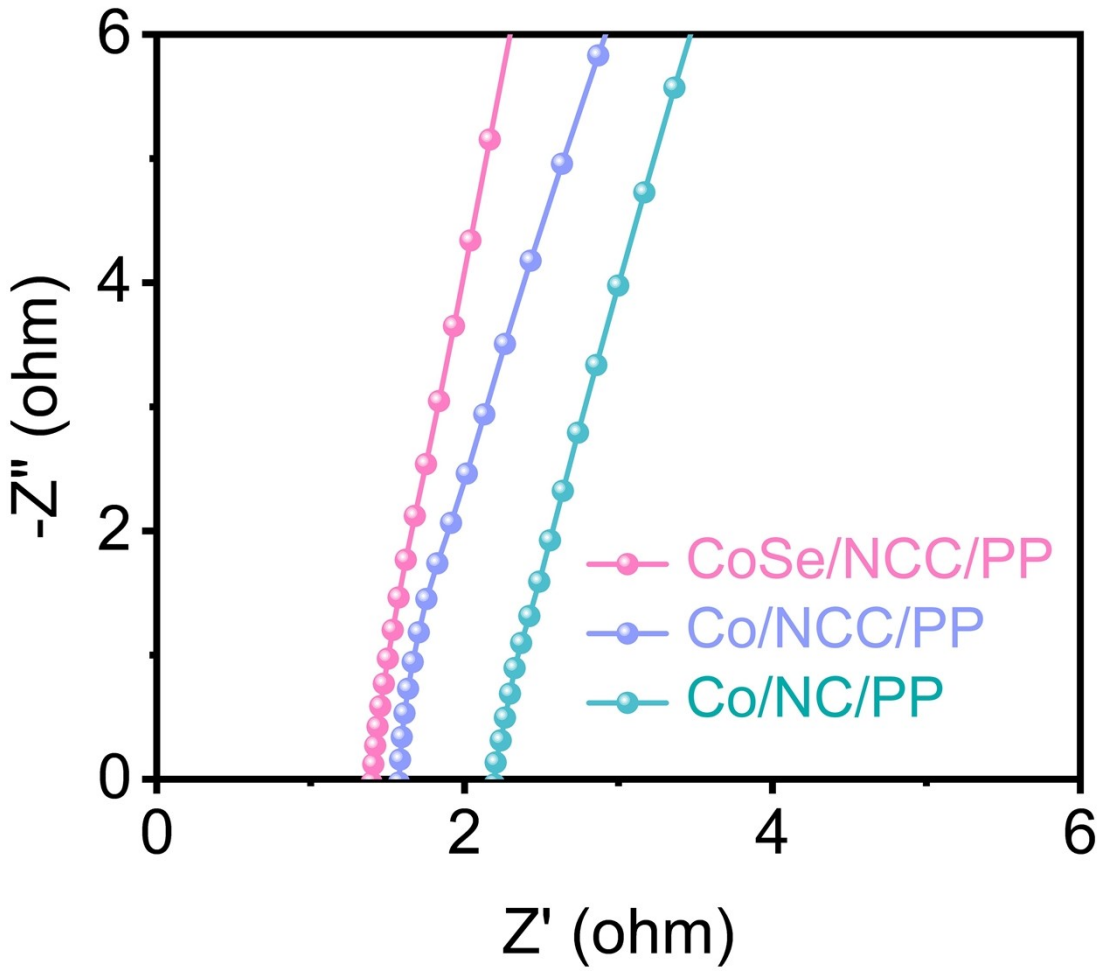

Figure S19 EIS spectra of symmetrical cells containing CoSe/NCC/PP, Co/NCC/PP, and Co/NC/PP separators.

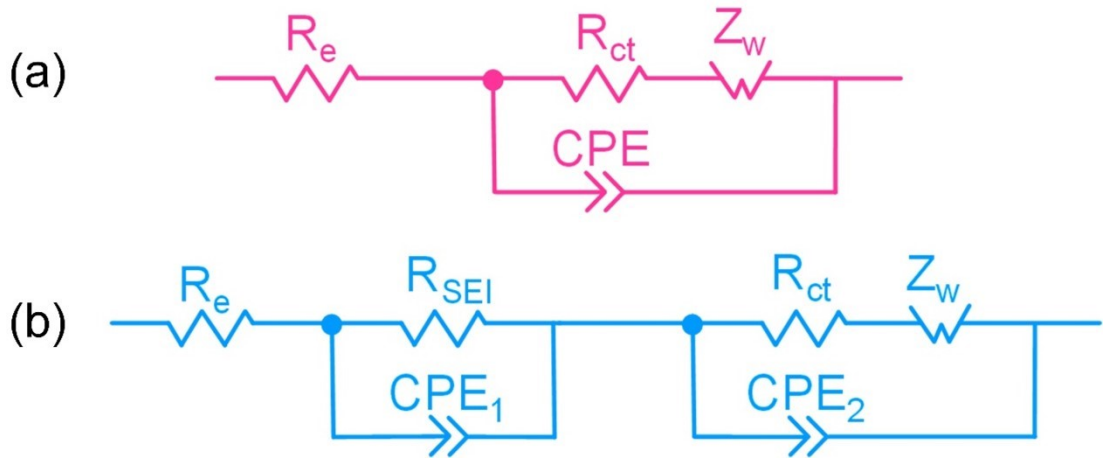

Figure S20 The equivalent circuits of LSBs (a) before cycling and (b) after 100 cycles.

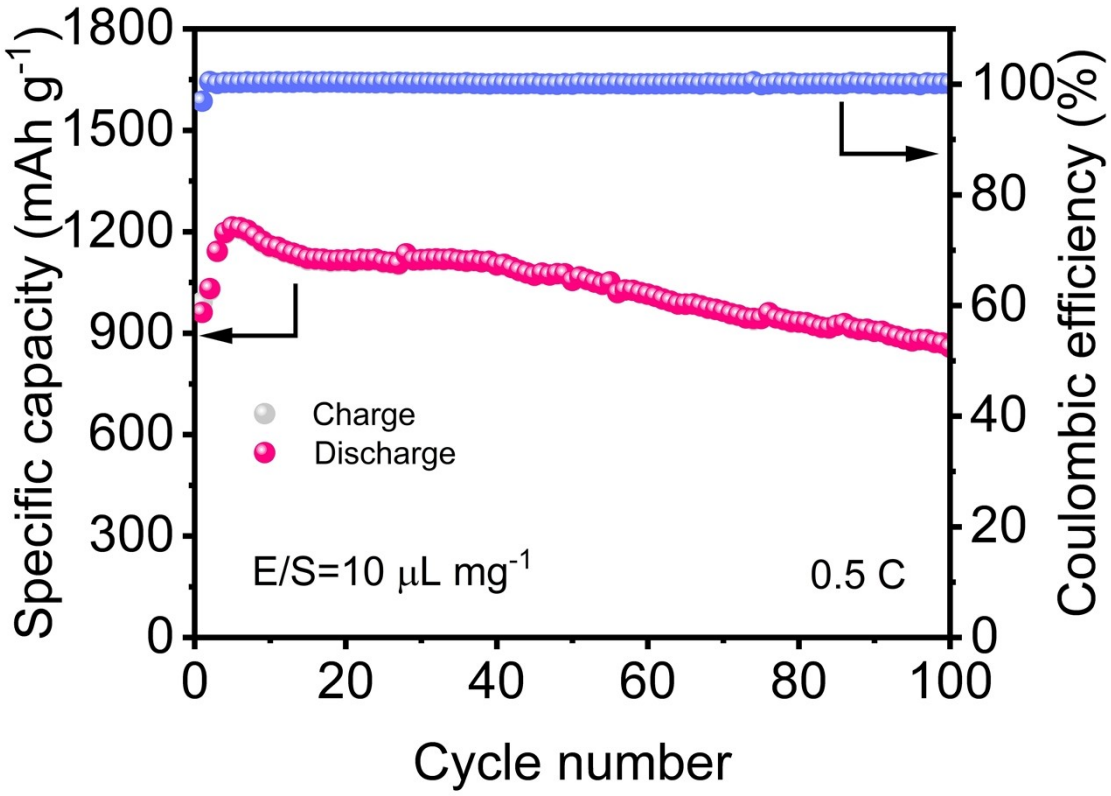

Figure S21 Cycling performance of lithium-sulfur battery with CoSe/NCC/PP separator under a E/S ratio of 10 μL mg^{-1} at 0.5 C.

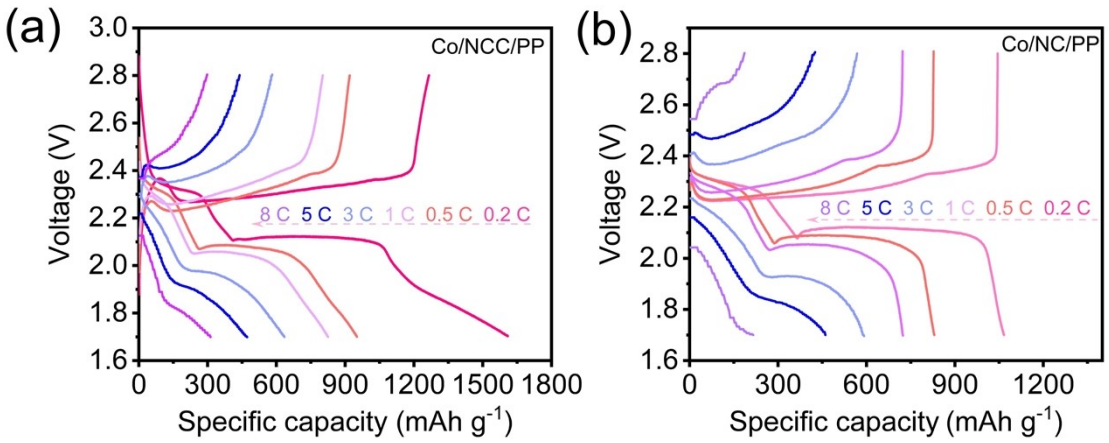

Figure S22 Galvanostatic charge-discharge curves of LSBs with (a) Co/NCC/PP and (b) Co/NC/PP separators at different current rates from 0.2-8 C.

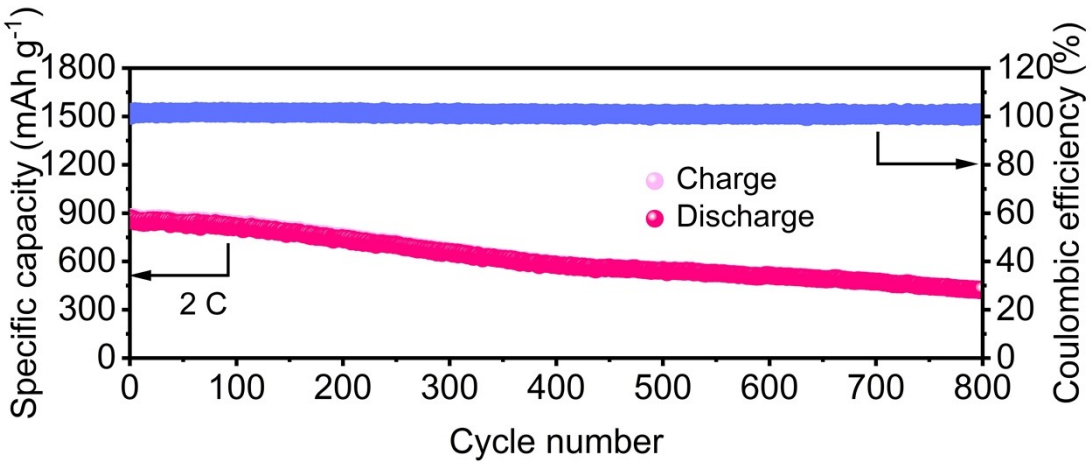

Figure S23 Cycling performance of lithium-sulfur battery with CoSe/NCC/PP separator at 2 C.

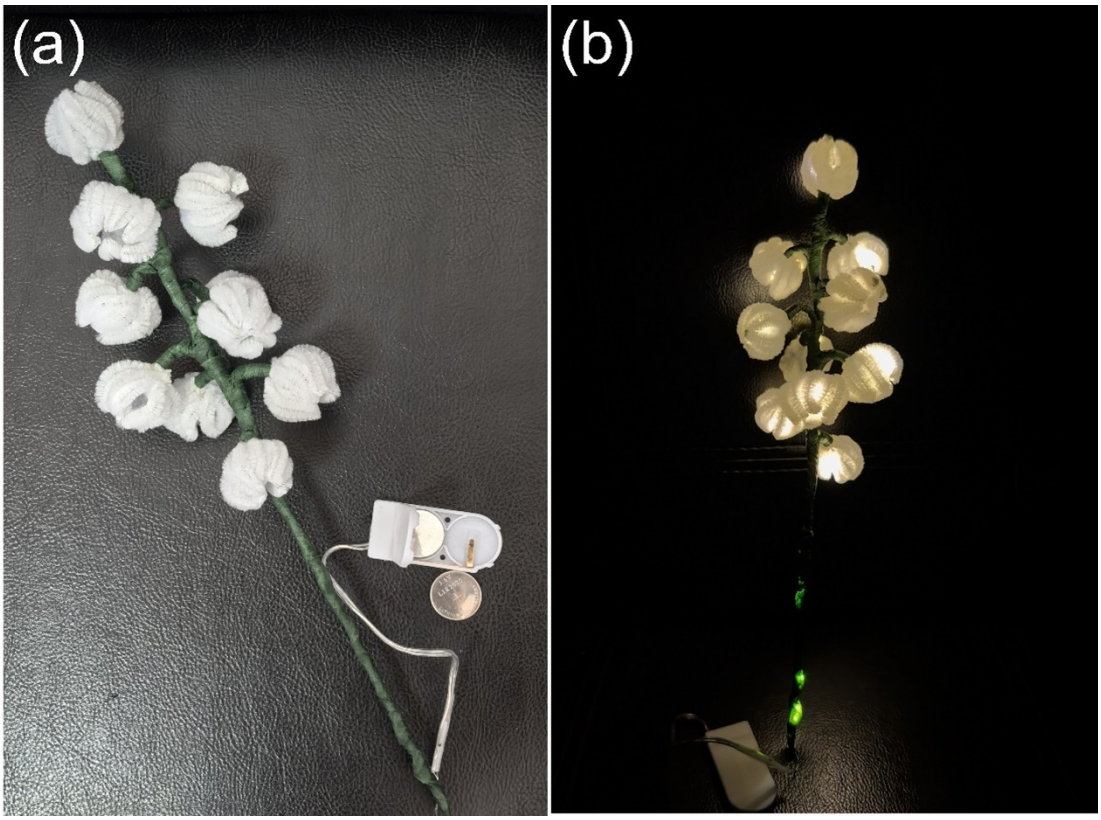

Figure S24 (a) Digital photo of a string of tulip flowers for ornamental value before light. (b) Digital photo of a string of tulip flowers for ornamental value lighted up by two LSBs with MWCNTs/S cathodes and CoSe/NCC/PP separators connected in series.

Table S1. Different fabrication parameters and key performance of LSBs.

Material	Sulfur content (%)	Sulfur loading (mg cm^{-2})	E/S ratio (μL mg^{-1})	Initial discharge capacity (mAh g^{-1}) (C-rate)
CoSe/NCC/PP+MWCNTs/S	72.7%	0.8	15	1270 (0.5 C) 874 (1 C) 869 (2 C) 572 (5 C)
		0.8	10	962 (0.5 C)
		1.1	13.6	1214 (0.2 C)
		2.0	7.5	452 (0.2 C)
		4.1	3.65	210 (0.2 C)
Co/NCC/PP+MWCNTs/S		0.8	15	1114 (0.5 C)
Co/NC/PP+MWCNTs/S		0.8	15	1008 (0.5 C)

Note: the mass of lithium is 48.4 mg.

Table S2 Comparison of lithium-sulfur battery assembled by MWCNTs/S+CoSe/NCC/PP with other published literatures.

Sulfur cathode	Modified separator material	Sulfur content (%)	Initial discharge capacity (mAh g^{-1})	Discharge Capacity (mAh g^{-1}) (Cycles, C-rate)	Capacity decay rate per cycle (%)	Ref.
Super P/S	$Ni_3(HITP)_2$	60	900	585 (300, 0.5 C)	0.12	S1
Super P/S	$NiCo_2S_4$@C	75	1000	830 (100, 0.5 C)	0.17	S2
S/CB	PVDF/PSSLi	-	955	446 (200, 0.5 C)	0.27	S3
CB-S	Oli/OAPS-PMIA	85	851	458 (800, 0.5 C)	0.057	S4
S/CB	PPy	70	934	517 (250, 0.5 C)	0.18	S5
S/CB	T@LPP	73.27	726	700 (200, 1 C)	0.018	S6
S/Super P	P2W18/PVDF	70	872	681 (300,1 C)	0.07	S7
ZnCoFe-NC/S	-	-	1062	751 (400, 1 C)	0.073	S8
Co-N-GC/S	-	-	1150	625 (500, 1 C)	0.091	S9
S/CNT	Fe_3Se_4@ PNCNFs	-	939	592 (500, 1 C)	0.074	S10
MWCNTs/S	**CoSe/NCC**	**72.7**	**1270**	**932 (100, 0.5 C)**	**0.266**	**This work**
			874	**648 (500, 1 C)**	**0.051**	

Notes and references

S1 H. H. Chen, Y. W. Xiao, C. Chen, J. Y. Yang, C. Gao, Y. S. Chen, J. S. Wu, Y.

Shen, W. N. Zhang, S. Li, F. W. Huo, B. Zheng, Conductive MOF-modified separator for mitigating the shuttle effect of lithium-sulfur battery through a filtration method, *ACS Appl. Mater. Interfaces* 2019, **11**, 11459-11465.

S2 B. H. Li, Y. X. Pan, B. Luo, J. Zao, Y. H. Xiao, S. J. Lei, B. C. Cheng, MOF-derived $NiCo_2S_4$@C as a separator modification material for high-performance lithium-sulfur batteries, *Electrochim. Acta* 2020, **344**, 135811.

S3 Y. S. Lin, R. Pitcheri, J. H. Zhu, C. M. Jiao, Y. Guo, J. Li, Y. J. Qiu, Electrospun PVDF/PSSLi ionomer films as a functional separator for lithium-sulfur batteries, *J. Alloy. Compd.* 2019, **785**, 627-633.

S4 H. J. Zhao, N. P. Deng, W. M. Kang, G. Wang, Y. Hao, Y. F. Zhang, B. W. Cheng, The significant effect of octa (aminophenyl) silsesquioxane on the electrospun ion-selective and ultra-strong poly-m-phenyleneisophthalamide separator for enhanced electrochemical performance of lithium-sulfur battery, *Chem. Eng. J.* 2020, **381**, 122715.

S5 Y. J. Li, W. Y. Wang, X. X. Liu, E. Mao, M. T. Wang, G. C. Li, L. Fu, Z. Li, A. Y. S. Eng, Z. W. Seh, Y. M. Sun, Engineering stable electrode-separator interfaces with ultrathin conductive polymer layer for high-energy-density Li-S batteries, *Energy Storage Mater.* 2019, **23**, 261-268.

S6 F. Lan, H. Zhang, J. Fan, Q. Xu, H. Li, Y. Min, Electrospun polymer nanofibers with TiO_2@NiCo-LDH as efficient polysulfide barriers for wide-temperature-range Li-S batteries, *ACS Appl. Mater. Interfaces* 2021, **13**, 2734-2744.

S7 H. Y. Zhang, Z. Y. Ma, S. Q. Duan, Y. Liu, X. Y. Jiang, Q. P. Zhou, M. Chen, L.

B. Ni, G. W. Diao, Dawson-type polyoxometalate modified separator for anchoring/catalyzing polysulfides in high-performance lithium-sulfur batteries, *Electrochim. Acta* 2022, **428**, 140868.

S8 X. Zhou, X. L. Huang, G. Li, P. Zeng, X. L. Liu, H. Liu, M. F. Chen, X. Y. Wang, An advanced SRR catalyst based on hollow polyhedral carbon skeleton modified by tri-metal (Zn, Co, Fe) for Li-S batteries, *Chem. Eng. J.* 2023, **471**, 144806.

S9 Y. J. Li, J. M. Fan, M.S. Zheng, Q. F. Dong, A novel synergistic composite with multi-functional effects for high-performance Li-S batteries, *Energ. Environ. Sci.* 2016, **9**, 1998-2004.

S10 Y. H. Lin, L. H. Li, L. J. Tan, Y. L. Li, X. Z. Ren, P. X. Zhang, C. X. He, L. N. Sun, Accelerating lithium-sulfur battery reaction kinetics and inducing 3D deposition of Li_2S using interactions between Fe_3Se_4 and lithium polysulfides, *Chem. Eng. J.* 2024, **95**, 540-553.